Solving Mad Dog subsalt imaging in two decades: From WATS to OBN to elastic FWI

Hui Liu[1], Fran Rollins[1], Kevin Pratt[1], Elizabeth Da Silva[1], Nathalie Mootoo[1], Tongning Yang[1], Dorothy Ren[2], Fei Gao[2], and Jiawei Mei[2]

https://doi.org/10.1190/tle42060398.1

Abstract

The Gulf of Mexico (GoM) is one of the most prolific oil and gas producing provinces in the world. The Mad Dog Field, like many large deepwater fields in the GoM, is subsalt. The geometric complexity of the overlying salt causes extremely variable image quality of the strata beneath the salt. Improving the seismic image has been critical for field development, and a tremendous amount of effort has been expended over the years to solve this problem. Over the past two decades, data acquisition has evolved from narrow-azimuth towed streamer to wide-azimuth streamer, and finally to ocean-bottom nodes. Processing methods such as using different anisotropic velocity models of increasing complexity, exhaustive iterations of salt modeling, acoustic full-waveform inversion, and most recently elastic full-waveform inversion have been applied. Dozens of wells have been drilled at Mad Dog guided by the resulting seismic images, and many acquisition and processing learnings have been acquired and implemented over this period to optimize the imaging. This paper explores the techniques that have caused major uplift to subsalt imaging and some techniques that were of only minor impact, while giving a glimpse into the imaging history of one of the GoM's giant fields.

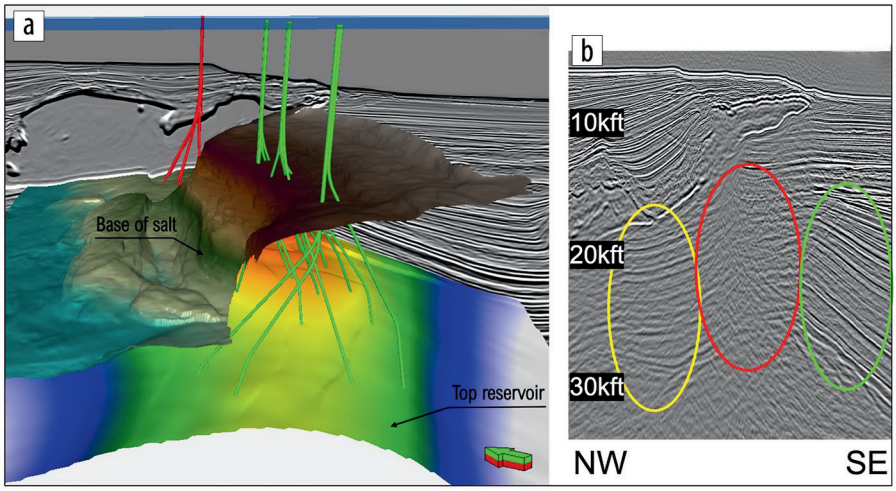

Figure 1. (a) Three-dimensional view of the Mad Dog Field with base of salt and top reservoir surface. Spar producers are in red, and MD2 wells are in green. The seismic image in the background is a northwest–southeast line in the eastern area of the Mad Dog Field. (b) Central northwest–southeast line of wave-equation migration of dual-azimuth NATS data sets. Black is a peak and white is a trough. The three ellipses show the image quality: green is good, yellow is fair, and red is poor.

Introduction

Mad Dog is a giant hydrocarbon field in the Gulf of Mexico (GoM) with an estimated 6 billion barrels of oil originally in place. It is located in the Green Canyon protraction area about 150 miles south of New Orleans and is co-owned by BP (60.5%), Woodside Energy (23.9%), and Chevron (15.6%). The field lies underneath the Sigsbee Escarpment, and water depths range from about 4100 ft to more than 6000 ft. Mad Dog is a large anticlinal structure in the western part of the Atwater Fold Belt. Most of the field is located beneath an allochthonous salt canopy of variable thickness. The maximum salt thickness is about 8000 ft.

Mad Dog was discovered in 1998 utilizing a Kirchhoff prestack depth-migrated narrow-azimuth towed-streamer (NATS) seismic data set. Around 2000, some wave-equation-based migration techniques were applied with very limited improvement. When first oil was achieved in 2005 through a floating spar facility, the field was poorly understood due to difficulties in imaging through the salt overburden and limited well control. As data quality improved in the following years, several additional appraisal wells were drilled to the north, west, and south, and it was realized that the field was much larger than originally estimated. This led to the sanctioning of Mad Dog Phase 2 (MD2) in 2016, which required a second, larger production facility.

Figure 1a shows a 3D view of the Mad Dog Field. Present production is from nine wells (in red) produced through the original spar platform. The Argos semisubmersible platform has been delivered and is presently being readied for MD2 production and injection from a series of predrilled wells (in green). The base of salt surface is overlain on the figure, demonstrating that all of the wells are drilled through salt. The base also shows complexity, with relatively flat surfaces in the northwest and a very steep salt face over the central portion of the field. This steep face has been the main impediment to getting a clear subsalt image and unfortunately is coincident with the general crest of the field structure.

Figure 1b shows a typical northwest–southeast cross section from a 2003 vintage processing of dual-azimuth NATS data (Michell et al., 2006); the subsalt image is poorest in the central

[1]BP, Houston, Texas, USA. E-mail: hui.liu@bp.com; francis.rollins@bp.com; kevin.pratt@bp.com; elizabeth.dasilva1@bp.com; nathalie.mootoo@bp.com; tongning.yang@bp.com.
[2]CGG, Houston, Texas, USA. E-mail: dorothy.ren@cgg.com; fei.gao@cgg.com; jiawei.mei@cgg.com.

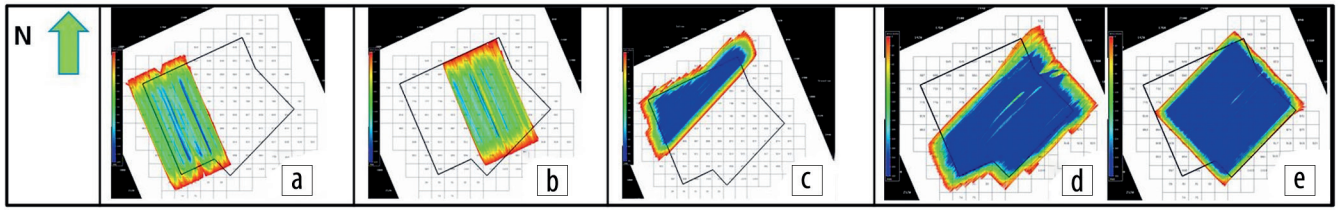

Figure 2. WATS surveys covering the Mad Dog area. The black polygon is the Mad Dog processing area of interest. The maps show the coverage and different sailing directions. Cooler colors indicate relatively higher fold.

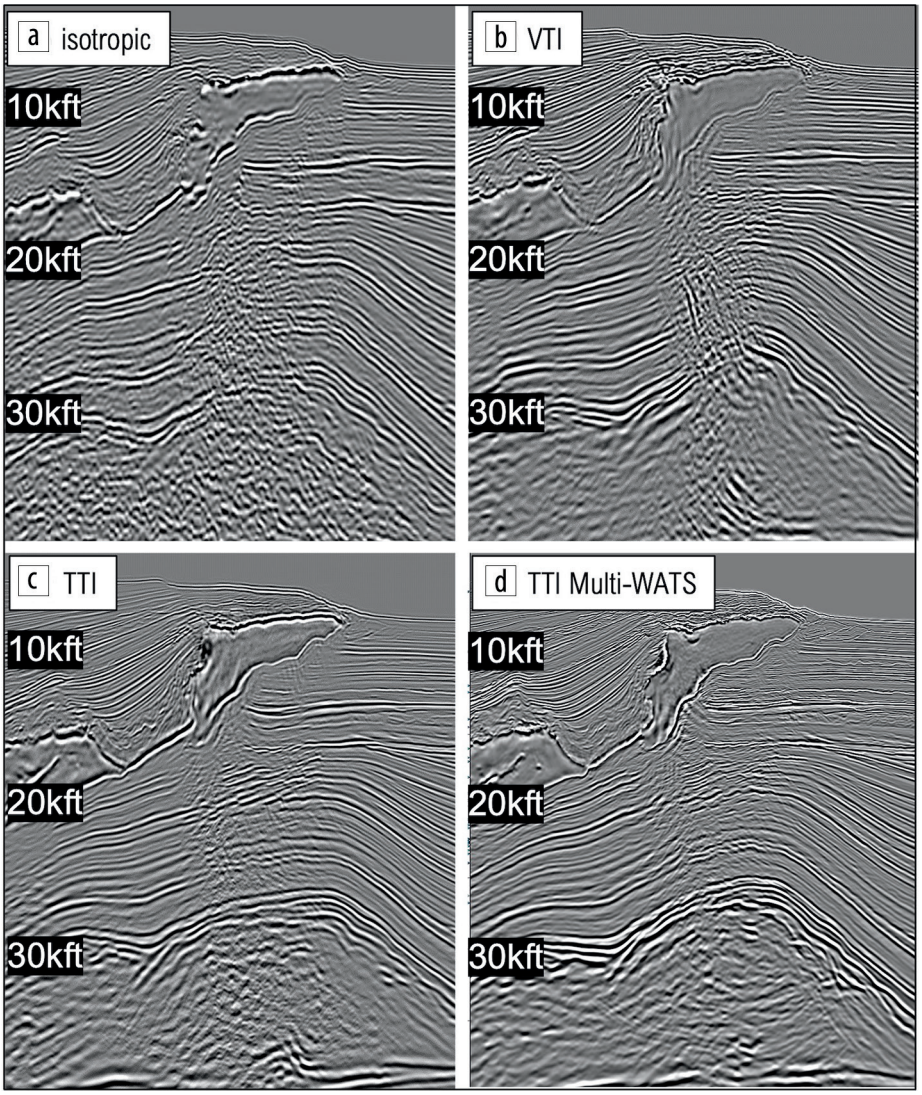

Figure 3. Central northwest–southeast line of RTM full-stack images migrating Mad Dog WATS data set with (a) isotropic velocity model in 2005, with (b) VTI models in 2007, with (c) TTI models in 2009, and (d) migrating multiple WATS data sets with TTI models in 2012. In all seismic images, black is a peak and white is a trough.

area of the line beneath the steep salt flank (red ellipse), while the northwest flank of the field has a fair image (yellow ellipse) due to relatively simple overlying salt. The image of the southeast flank of the field is of good quality (green ellipse) where there is no overburden salt. However, approximately 85% of the reservoir area is subsalt, and most drilled wells and future drilling targets are in the area of the red ellipse. Without further image improvement, Mad Dog development would have been hampered severely.

The cross section shown in Figure 1b will be used frequently in the later sections of this paper for comparison to show the imaging progression.

Wide-azimuth towed streamer

It became obvious that narrow-azimuth seismic data were not going to provide a sufficient imaging solution for Mad Dog. Therefore, BP and co-owners looked for a new way to acquire better data. Seismic acquisition modeling suggested that wide-azimuth acquisition could fill in illumination holes and provide a better subsalt image. In late 2004, the world's first large-scale wide-azimuth towed-streamer (WATS) survey was acquired at Mad Dog (Figures 2a and 2b). The first WATS reverse time migration (RTM) image (Figure 3a) demonstrated that the WATS acquisition with better azimuthal coverage provided better subsurface illumination beneath salt, better suppression of multiple energy, and a greatly improved overall image (Michell et al., 2006). Since the WATS modeling work (Regone, 2006) and the imaging uplift from the Mad Dog WATS survey were shared with the industry, additional speculative WATS surveys over the Mad Dog area with different sailing directions (Figures 2c–2e) were acquired over the following years.

Interpretation-based velocity model building and anisotropy

At the time the Mad Dog WATS surveys were acquired, velocity models for the GoM typically were built with a sequential workflow: water flood, water bottom picking, sediment flood, top of salt picking, salt flood, base of salt picking, and then subsalt sediment updating. Usually, the areas having complex salt required picking of multiple salt tops and bases and several salt scenario tests. This interpretation-intensive workflow usually required a large project team, frequent QC meetings, and months of cycle time. It was commonly true that

the quality of velocity model building (VMB) and imaging were highly dependent on the effort and experience of the project team members.

Around the same time, different methods to account for various anisotropic models became available. Mad Dog utilized the advances in the technology in successive processing projects. In 2007, vertical transverse isotropy (VTI) VMB and imaging (Figure 3b), along with the painstaking salt model reconstruction, demonstrated superior imaging ability over the isotropic processing in terms of better spatial positioning (Bowling et al., 2009). In 2009, tilted transverse isotropy (TTI) VMB and imaging (Figure 3c), which allowed the orientation of the anisotropic symmetry axis to follow structural dip, positioned steep salt boundaries better and resulted in further improvement of imaging (Bowling et al., 2009, 2010).

As encouraged by the 2009 TTI project, a second TTI processing project was performed, combining all the available WATS data sets and including older NATS surveys for the dense near-offset fold (Rollins et al., 2013). Better illumination and constraints for VMB resulted in a better subsalt image (Figure 3d). Although most of the uplift has been attributed to the multi-WATS input, additional processing techniques, such as dirty salt inversion, were also applied and further enhanced the image.

In 2016, tilted orthorhombic (TOR) anisotropy was applied to the suprasalt region where gather signal quality was sufficient to pick the curvature residual necessary for the orthorhombic VMB. This provided a slightly better top of salt model and correspondingly an improved salt flood and subsalt VMB based on the continued learnings from previous projects (Dadi et al., 2018). The TOR RTM is considered the best WATS image and will be used to compare with ocean-bottom node (OBN) images in the latter part of this paper (Figures 5–7).

Although different types of anisotropy, iterations of salt scenario testing, and a series of technological advances have provided continued improvement of the subsalt imaging, image improvement and processing outcomes had reached a technical limit. The legacy multi-WATS imaging and finite-difference modeling suggested that better azimuthal coverage can significantly improve imaging. At this point, examples of full-waveform inversion (FWI) along with OBN acquisition with long offsets, full-azimuth coverage, and rich lower frequencies promised step-change improvements in imaging (Shen et al., 2017), which spurred Mad Dog to pursue OBN.

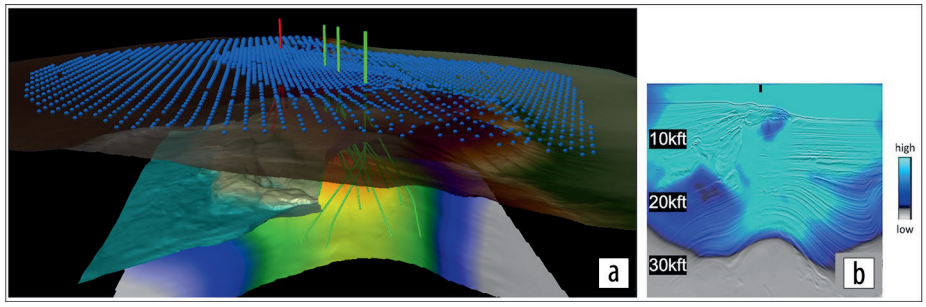

Figure 4. (a) Three-dimensional view of the Mad Dog Field with OBNs (in blue dots), overlaid with water bottom, base of salt, top reservoir surfaces, Spar producers (in red trajectories), and MD2 wells (in green trajectories). (b) Diving wave illumination section, with a color bar showing the variation of the illumination.

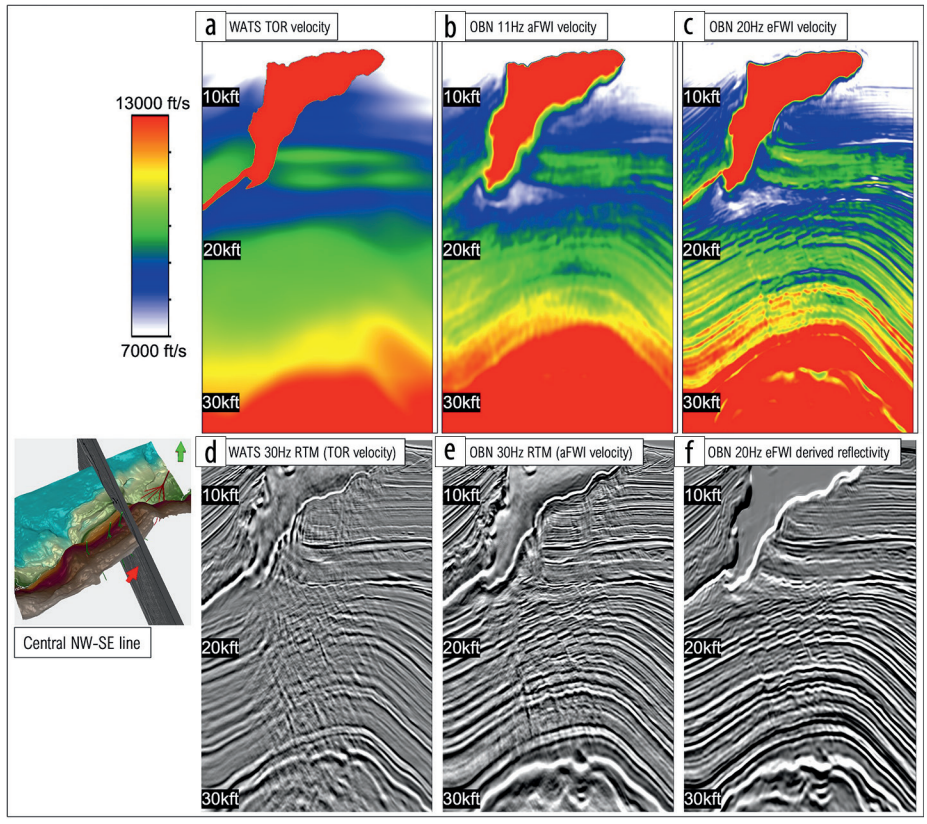

Figure 5. Central northwest–southeast cross section. A 3D map view at the left side shows the location. (a) WATS TOR velocity model. (b) OBN 11 Hz A-FWI velocity model. (c) OBN 20 Hz E-FWI velocity model. (d) 30 Hz WATS RTM full-stack image migrated with TOR model. (e) 30 Hz OBN RTM full-stack image migrated with A-FWI model. (f) 20 Hz E-FWI-derived reflectivity. In all seismic images, black is a peak and white is a trough.

OBN and FWI

The first OBN survey at Mad Dog was acquired in early 2018 with a patch of densely spaced nodes (213 × 369 m) over the core of the Mad Dog structure and a conventional spacing (427 × 369 m) over the rest of the field (as shown in Figure 4a). Because FWI primarily uses diving wave energy to invert for the velocity model, the Mad Dog OBN survey was designed to have minimum offsets of 10–12 km, with maximum offsets more than 20 km, which

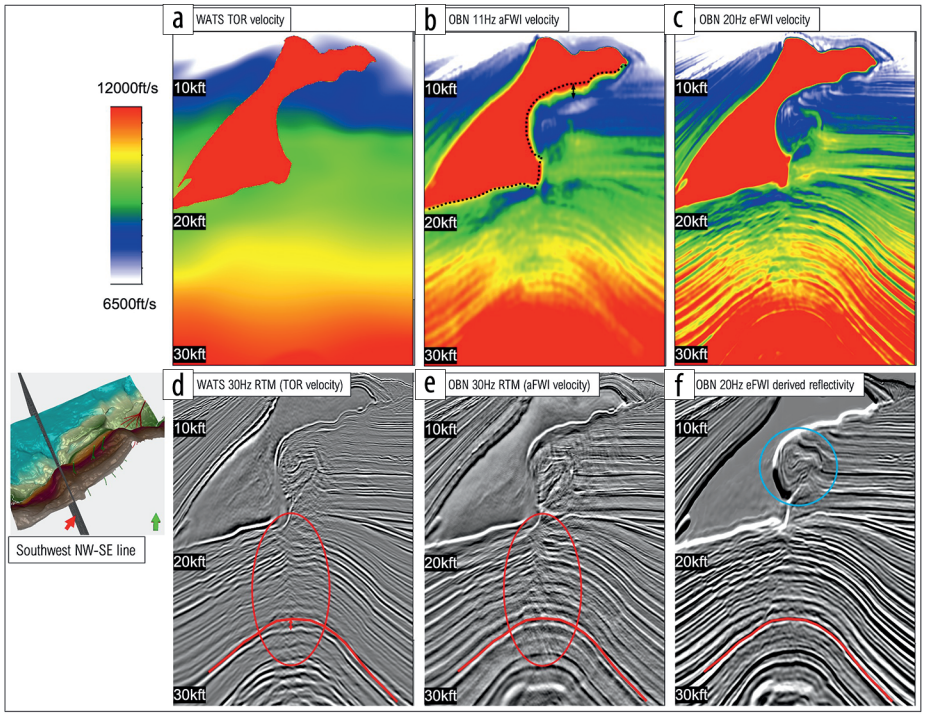

Figure 6. Southwest northwest–southeast cross section. A 3D map view at the left side shows the location. (a) WATS TOR velocity model. (b) OBN 11 Hz A-FWI velocity model. (c) OBN 20 Hz E-FWI velocity model. (d) 30 Hz WATS RTM full-stack image migrated with TOR model. (e) 30 Hz OBN RTM full-stack image migrated with A-FWI model. (f) 20 Hz E-FWI-derived reflectivity. In all seismic images, black is a peak and white is a trough.

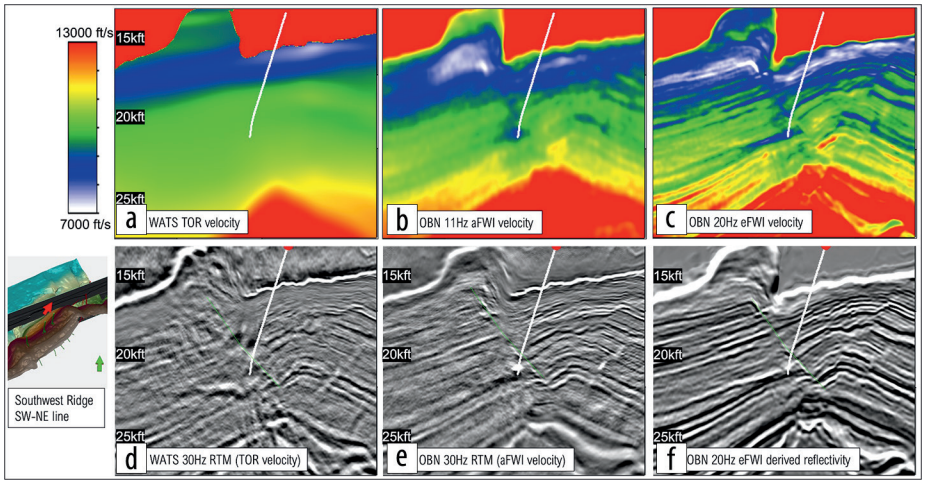

Figure 7. Southwest Ridge southwest–northeast cross section. A 3D map view at the left side shows the location. The white trajectory is A5 producer. The green polyline is the interpreted graben sealing fault. (a) WATS TOR velocity model. (b) OBN 11 Hz A-FWI velocity model. (c) OBN 20 Hz E-FWI velocity model. (d) 30 Hz WATS RTM full-stack image migrated with TOR model. (e) 30 Hz OBN RTM full-stack image migrated with A-FWI model. (f) 20 Hz E-FWI-derived reflectivity. In all seismic images, black is a peak and white is a trough.

made it very suitable for FWI application. An illumination study confirmed that the reservoir level would be penetrated by the diving waves and updated through FWI (Figure 4b).

FWI as a data-driven approach can be run as a standalone modeling tool to update the velocity automatically, even with limited tomographic updating of the anisotropy parameters. This is revolutionary, as several iterations of water, sediment, and salt floods, and manual picking of the top and base salt horizons were no longer necessary, which significantly shortened the VMB turnaround time. Furthermore, the complex salt geometry and velocity resolved by FWI is almost impossible to obtain through manual interpretation. As a result, a greatly improved image can be obtained a few months after the end of the acquisition. After that, processing time is focused on depth corrections and other optimizations instead of seemingly endless scenario testing. This was the first time that the tedious interpretation-based VMB process was not used at Mad Dog (Nolte et al., 2019). OBN RTM with FWI velocity model was a step change in imaging quality compared to WATS RTM and will be shown in comparisons later (Figures 5–7).

Elastic FWI and derived reflectivity

Since late 2020, FWI imaging has emerged (Huang et al., 2021) that uses the full wavefield to invert for the velocity and then derives the reflectivity from the velocity model. Recently, elastic FWI (E-FWI) applications in the GoM have been promising (Elebiju et al., 2022; Wu et al., 2022), and this is an area of continued research. E-FWI simulates elastic wave propagation in the subsurface and thus can better handle the reflection energies beyond the critical angle and the converted wave energy around sharp velocity contrasts. The effective reduction of the salt halo by E-FWI not only provides a better definition of the salt geometry but also helps focus the energy subsalt, which is the key to inverting for higher frequencies.

In 2022, E-FWI was applied to the Mad Dog OBN data set with deliverables including the velocity model and the E-FWI-derived image. To avoid unstable multiparameter inversion, E-FWI only inverted for the P-wave velocity and updated the S-wave velocity using a simple empirical relationship. A constant density model was used, and density was held fixed throughout the inversion process. This simplification of the model parameterization provides a trade-off between elastic representation of the subsurface and the necessary constraints in the inversion.

To provide a detailed comparison between the WATS RTM with TOR model, OBN RTM with acoustic FWI (A-FWI) model, and the latest E-FWI image, three locations are selected: the central northwest–southeast line (the same line shown in Figure 1b and

Figure 3), a Southwest northwest–southeast line, and a Southwest Ridge southwest–northeast crossline. The latter two locations are in areas that are poorly illuminated by primary reflections.

Figure 5 shows the central northwest–southeast cross section. The TOR velocity model (Figure 5a) was generated by the top-down interpretation-based VMB workflow. Due to the inaccurate velocities, the WATS RTM image (Figure 5d) was not focused and had poor horizon continuity. Poorly resolved fault planes and high-dip imaging artifacts conflicted with each other, making interpretation difficult. The OBN A-FWI automatically inverted the velocity (Figure 5b) for the salt structure and the sediment with a precision that better focused the RTM imaging (Figure 5e). The fault planes were well defined, and horizon continuity was improved over most of the section. The OBN data have a higher signal-to-noise ratio (S/N), and the extended lower frequencies provide a richer seismic character for interpretation.

Traditional RTM imaging outputs are seismic migrations in the reflectivity domain, and the industry must use different kinds of inversion techniques to invert the reflectivity to layer properties. The latest 20 Hz OBN E-FWI model (Figure 5c) has dramatic resolution improvements with crisp velocity contrast between the fault blocks. It shows the potential for direct interpretation on the model. In the reflectivity domain, the E-FWI-derived image (Figure 5f) shows higher S/N, clearer fault truncations, and better reflector continuity than a conventional RTM image.

At this central area of the field with complex overlaying salt, the OBN RTM image with A-FWI model showed a step change from the previous WATS RTM image and was largely appropriate for field development. But there were still areas in the field — the Southwest and Southwest Ridge areas — where more complex salt geometry continued to plague attempts to give a clear OBN RTM image.

Figure 6 shows the Southwest northwest–southeast line where the WATS RTM (Figure 6d) with TOR velocity (Figure 6a) had a very poor subsalt image (in red ellipse). The OBN RTM (Figure 6e) with A-FWI model (Figure 6b) has improved but still suffers from imaging artifacts (in red ellipse) caused by the complex overburden. The E-FWI resolved the complex velocity model (Figure 6c) and significantly improved the subsalt image quality (Figure 6f) with much better focusing and higher S/N. The E-FWI-derived reflectivity shows that this area is highly compartmentalized, which is confirmed by a well drilled into this area in the past. This new image will largely reduce the uncertainty for future well targeting and planning.

In the A-FWI model (Figure 6b), the base of salt is overlaid as a dashed polyline. It shows clearly that the A-FWI model has a large salt halo by averaging the velocity field around the salt body, so no longer was there a sharp salt boundary as would be created with the conventional interpretation-based salt picking. The black bar shows the salt halo where it is about 500 ft thick. The main reason behind the large salt halo in the A-FWI velocity model is because A-FWI cannot properly model strong elastic effects around salt boundaries with large impedance contrasts; this halo does not shrink properly when the A-FWI goes to higher frequencies. The salt halo makes A-FWI velocities not only inappropriate for pressure prediction close to salt boundaries but also limits the ability of interpreters to give a precise estimation of salt depth for well planning. By reducing the mismatch between the recorded data and the synthetic, which was generated with an elastic wave propagation engine to better simulate the phase and amplitudes of the reflection and transmission energy at salt boundaries, E-FWI was able to effectively reduce the salt halo and sharpen the salt boundary (as shown in Figure 6c).

The blue circle in Figure 6f clearly shows a geobody in the overburden characterized by very complex sediment and salt interaction. The team has struggled with this feature for years, and many migration scenario tests were conducted to try to resolve the character of this feature — with little success. This overburden area in the TOR model above the crest of the structure prevented clear imaging and depth prediction due to the inability to properly characterize it in the velocity model. Also, the noise caused by the improperly resolved geobody impacted the ability to interpret faulting in the area. The red horizons (in Figures 6d–6f) are the top reservoir. The red bar in Figure 6d shows that the imaged top reservoir structure was too deep by missing the low-velocity geobody in the TOR velocity model.

The OBN A-FWI velocity model largely solved the low-velocity geobody and positioned the top reservoir event roughly at the right depth, but the OBN RTM image quality in the red ellipse (in Figure 6e) was still poor. The main reason is that the primary reflection energy poorly illuminates this area. To further demonstrate, Figure 7 shows a southwest–northeast crossline through the poorly imaged Southwest Ridge area. This cross section lies right along the steep salt face, so the whole line of the WATS RTM image (Figure 7d) was very poor. The producer A5 (in white) targeted the reservoir updip near a major graben sealing fault (in dashed green line) that was poorly defined on the image. Compared to the WATS RTM image, the OBN RTM (Figure 7e) migrated with A-FWI velocity model (Figure 7b) showed some improvement because of better azimuth and offset coverage of the OBN acquisition. With the improved illumination and S/N from the iterative least-squares fitting of full wavefield data in E-FWI, the whole section in E-FWI-derived reflectivity (Figure 7f) is much cleaner and crisper, and the graben fault is easier to interpret. As a direct impact of the E-FWI, a new well target close to this area was identified due to less structural uncertainty.

To further QC the inverted velocity, sonic logs were compared with the velocity extractions from the A-FWI and E-FWI models (Figure 8). For a fair comparison, both A-FWI (in yellow) and E-FWI (in red) are 15 Hz; the velocity in the E-FWI model matches the sonic log much better, which supports that E-FWI is more robust in VMB and imaging. The large salt halo in the A-FWI model can also be observed in these plots. The E-FWI velocity around the salt does not suffer from the halo artifact and closely matches the sonic logs, which makes it a better candidate for pressure prediction.

In a recent well planning activity, the OBN RTM (migrated with A-FWI velocity) and the 20 Hz E-FWI image were compared and evaluated to scope the well trajectory. The drilling results showed that the E-FWI better identified the lithologic sequences, all surfaces came within prognosis, and no unexpected faults were intersected in the section. Misties for this well and most of the

legacy wells are less than 50 ft with a couple of outliers around 100 ft. This is deemed quite good considering the depth to target is in excess of 20,000 ft.

Progression of interpretation

Since the discovery of Mad Dog Field, along with improve VMB and imaging, there have been numerous seismic interpretation updates. The progression of interpreted maps (Figure 9) has shown better understanding of the field over time, with a resultant evolution of development strategy. The interpreted structure was simple at the beginning (Figures 9a and 9b) due to the unimaged faults at the crest of the anticline structure in the subsalt image. With imaging improvement over time, more faults became visible and were interpreted. However, plenty of imaging artifacts caused by the complex salt in the overburden were also interpreted as faults. Fault density is highest in Figures 9c and 9d. In the OBN image migrated with A-FWI velocity model, the imaging artifacts were significantly reduced and many previously interpreted faults were removed (Figure 9e). The fault interpretation on the latest E-FWI is currently being refined, and we expect the complex Southwest and Southwest Ridge areas to have a more robust interpretation.

Cycle-time reduction

A conventional processing and imaging project in the GoM with salt structures includes preprocessing, interpretation-intensive VMB, migration, and postmigration enhancement, which typically takes well over a year. FWI using raw data dramatically reduces the time spent in the VMB, and the derived reflectivity from the E-FWI-inverted velocity model allows users to have access to subsurface images in a few months after the processing projects start.

At the interpretation stage, the high quality of the E-FWI velocity model and its derived reflectivity could be suitable for the application of some automated interpretation tools and allow for very rapid interpretation of the entire field, from seabed down to the base of the autochthonous salt. Products such as horizons/faults (Figure 10a), amplitude/velocity extractions, and spectral decompositions (Figure 10b) can be generated quickly and integrated into existing geologic scenarios for real-time drilling, identifying future targets, and maturing the static understanding of current producers.

When primary reflection imaging fails

It has been demonstrated that the E-FWI model provided high-resolution velocity details and a resolved subsalt image. However, the E-FWI-derived reflectivity does not output gathers, which limits prestack applications such as amplitude variation with offset. Can we take the E-FWI velocity model to migrate the OBN data sets through conventional imaging methods (which can output gathers) such as RTM, meanwhile achieving the desired imaging quality? Figure 11 shows that, in areas of poor illumination by primary reflection energy, a good quality image may not be possible with conventional reflection-based migration, even with a very high-quality velocity model. In this situation, E-FWI might solve the imaging using the full wavefield including reflections, diving waves, and multiples.

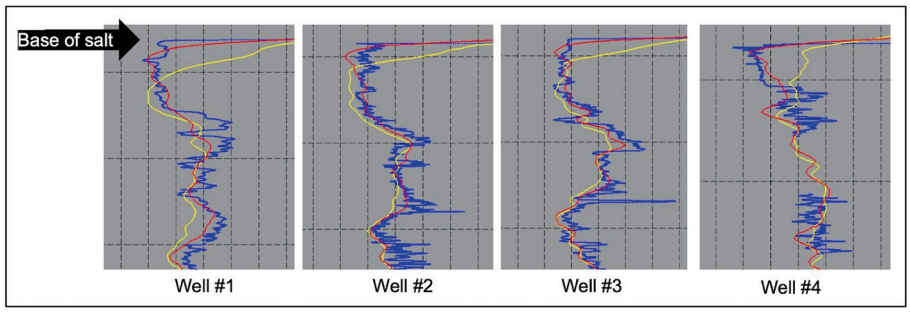

Figure 8. Velocity comparison for four wells. Sonic logs are in blue. 15 Hz E-FWI velocity curves are in red; 15 Hz A-FWI velocity curves are in yellow.

Conclusions and discussion

It has been two decades since the wave-equation depth-migrated image of dual-azimuth NATS data set (Figure 1b) was generated at Mad Dog. With the latest E-FWI image (Figure 5f), subsalt imaging at the field has been improved and the imaging quality is appropriate for field development. This paper shows how the subsalt imaging and interpretation have evolved over these 20 years, with the knowledge

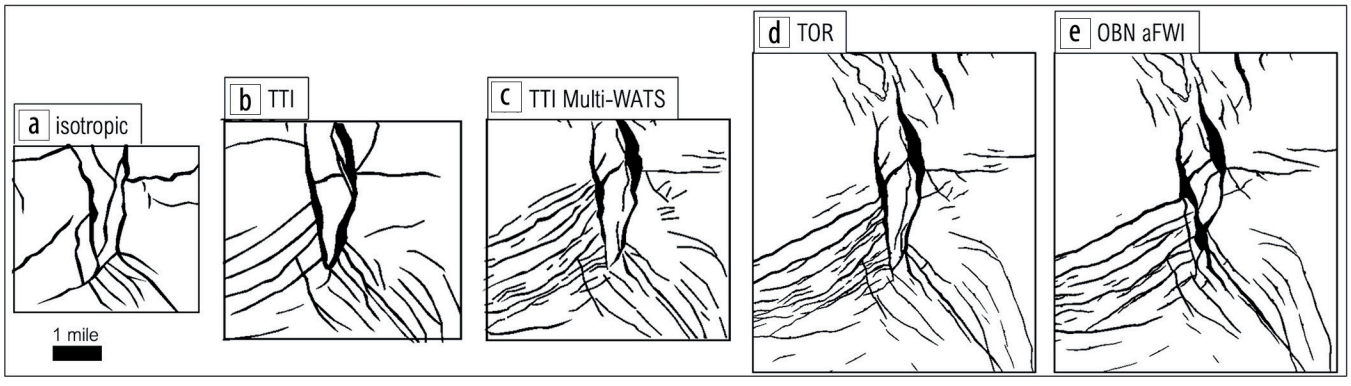

Figure 9. Faults interpretation on (a) 2005 isotropic RTM, (b) 2009 TTI RTM, (c) 2013 multi-WATS TTI RTM, (d) 2016 TOR RTM, and (e) 2018 OBN RTM migrated with A-FWI velocity.

gained at each stage driving the next phase of seismic acquisition and processing.

The first major subsalt imaging improvement was achieved by acquiring the WATS data set to gain more subsalt illumination and better constraints for VMB and imaging. For the subsalt target with simple overlaying salt structure, RTM migrating WATS data sets with interpretation-based VMB could generate a fair subsalt image. Different types of anisotropy in the legacy imaging projects have not only provided better image focusing and structural positioning, but also have led to an improved understanding of the subsurface and a quality initial model for A-FWI and later E-FWI.

For areas with complex overlaying salt structure, tens of iterations of salt scenario testing and a series of technological advances such as dirty salt inversion have generated incremental improvement but have never solved the subsalt imaging issues. After the OBN was acquired at Mad Dog, a step-change improvement in subsalt RTM image was achieved due to the better velocity model from A-FWI using the OBN data with the long-offset, full-azimuth, and rich low frequencies.

The third step change came from E-FWI, which can better model the strong elastic effects around salt boundaries with large impedance contrasts. Compared to the A-FWI model, the E-FWI model showed a reduced salt halo and an improved S/N as more recorded energies are better explained; the E-FWI also comparatively showed a better match to well logs. With these advantages of a sharp salt boundary definition, well-defined geologic layers, and clear fault truncations, the E-FWI model becomes more easily interpretable and a better candidate for pressure prediction. Compared to the RTM image, the E-FWI-derived reflectivity provided significant imaging uplift in the areas with very poor illumination of primary reflections, due to the additional illumination from the full wavefield, particularly diving waves and multiples. These comparisons have supported that the E-FWI products with sufficient bandwidth can be used as the primary interpretation volume for subsalt reservoirs.

E-FWI processing utilizes raw shot gathers as the input and directly outputs the model and image without pre- and postprocessing. The image quality is suitable for automated interpretation tools that can generate interpretations in weeks instead of months, resulting in cycle-time reduction.

The current E-FWI utilized a simple empirical relationship between P-wave and S-wave velocities as a priori information and a constant density model to reduce model parameters for better constraints in the inversion. Although the E-FWI velocity extractions along the wells match with the sonic better than A-FWI, some velocity details could come from density perturbations. Attention must be paid when the velocity model is directly used for detailed subsurface characterization. In the meantime, we do not have the traditional gather output from E-FWI for prestack applications. Despite these limitations, E-FWI has brought subsalt imaging to a new level. TLE

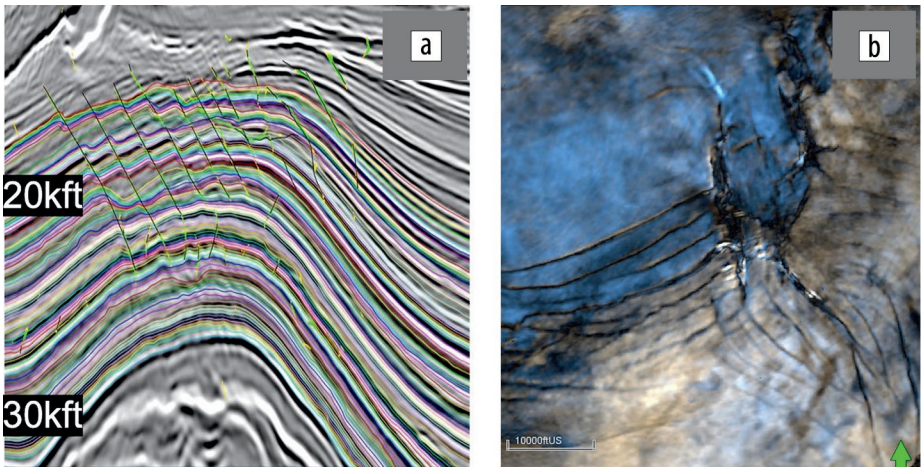

Figure 10. Products generated by rapid interpretation of E-FWI. (a) Central northwest–southeast line of E-FWI-derived reflectivity with isochronous horizons and faults picked by automated interpretation tools. (b) Example of RGB-blended spectral decomposition horizon slice in the overburden created using one of the horizons from (a) showing complex faulting patterns.

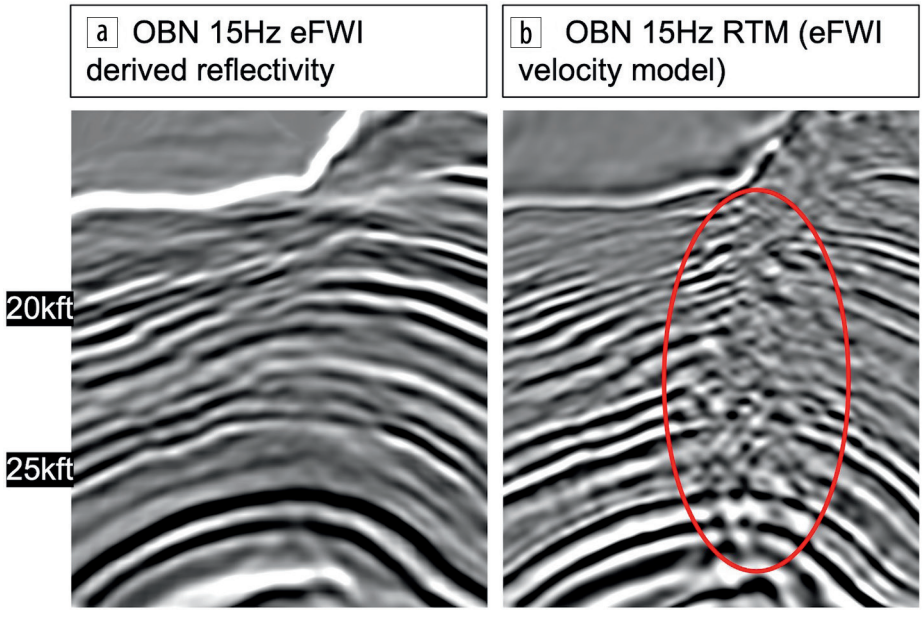

Figure 11. Southwestern northwest–southeast line of (a) 15 Hz E-FWI-derived reflectivity and (b) 15 Hz RTM full-stack image migrated with 15 Hz E-FWI velocity model. In both seismic images, black is a peak and white is a trough.

Acknowledgments

The authors would like to thank BP and co-owners, Woodside Energy and Chevron, for permission to publish this work and use the images showing Mad Dog proprietary seismic data. We also would like to thank CGG for their years of effort in data processing. We are grateful to current and former BP colleagues John Etgen, Andrew Cunningham, Frederic Billette, Carl Regone, Scott Michell, Jerry Bowling, Uwe Albertin, Bertram Nolte, Qingsong Li, Kang Fu, Pierre Ariston, and many others who have put significant effort into the modeling, acquisition design, and processing algorithms to help improve Mad Dog subsalt imaging in the past two decades. Lastly, we would like to thank Joshua Richardson, Greg Roche, and another anonymous reviewer for their great feedback and comments.

Data and materials availability

Data associated with this research are confidential and cannot be released.

Corresponding author: hui.liu@bp.com

References

Bowling, J., S. Ji, D. Lin, M. Reasnor, M. Staines, and N. Burke, 2009, From isotropic to anisotropic: Puma/Mad Dog wide azimuth data case study: 79th Annual International Meeting, SEG, Expanded Abstracts, 246–250, https://doi.org/10.1190/1.3255357.

Bowling, J., S. Ji, D. Lin, D. Chergotis, B. Nolte, and D. Yanchak, 2010, Mad Dog TTI RTM: Better than expected: 80th Annual International Meeting, SEG, Expanded Abstracts, 3313–3317, https://doi.org/10.1190/1.3513536.

Dadi, S., F. Rollins, K. Fu, N. Mootoo, Q. Sun, and W. Gou, 2018, From TTI to orthorhombic: A case study with multiple WATS/NATS at Mad Dog, Gulf of Mexico: 88th Annual International Meeting, SEG, Expanded Abstracts, 5152–5156, https://doi.org/10.1190/segam2018-2997390.1.

Elebiju, B., Q. Li, K. Hartman, F. Rollins, Y. Feng, K. Kaiser, W. Schinagl, C. Chen, Y. Hao, Z. Wei, and J. Mei, 2022, One more stride forward in Thunder Horse subsalt imaging with elastic FWI: Second International Meeting for Applied Geoscience & Energy, SEG/AAPG, Expanded Abstracts, 947–951, https://doi.org/10.1190/image2022-3750987.1.

Huang, R. Z., Z. Zhang, Z. Wu, Z. Wei, J. Mei, and P. Wang, 2021, Full-waveform inversion for full-wavefield imaging: Decades in the making: The Leading Edge, **40**, no. 5, 324–334, https://doi.org/10.1190/tle40050324.1.

Michell, S., E. Shoshitaishvili, D. Chergotis, J. Sharp, and J. Etgen, 2006, Wide azimuth streamer imaging of Mad Dog; have we solved the subsalt imaging problem?: 76th Annual International Meeting, SEG, Expanded Abstracts, 2905–2909, https://doi.org/10.1190/1.2370130.

Nolte, B., F. Rollins, Q. Li, S. Dadi, S. Yang, J. Mei, and R. Huang, 2019, Salt velocity model building with FWI on OBN data: Example from Mad Dog, Gulf of Mexico: 89th Annual International Meeting, SEG, Expanded Abstracts, 1275–1279, https://doi.org/10.1190/segam2019-3216777.1.

Regone, C., 2006, A modeling approach to wide-azimuth design for subsalt imaging: The Leading Edge, **25**, no. 12, 1467–1475, https://doi.org/10.1190/1.2405331.

Rollins, F., P.-O. Ariston, J. Bowling, W. Gou, S. Ji, and Y. Li, 2013, TTI imaging with multi-wide azimuth data — A case study at Mad Dog, GOM: 83rd Annual International Meeting, SEG, Expanded Abstracts, 3804–3809, https://doi.org/10.1190/segam2013-0720.1.

Shen, X., I. Ahmed, A. Brenders, J. Dellinger, J. Etgen, and S. Michell, 2017, Salt model building at Atlantis with full-waveform inversion: 87th Annual International Meeting, SEG, Expanded Abstracts, 1507–1511, https://doi.org/10.1190/segam2017-17738630.1.

Wu, Z., Z. Wei, Z. Zhang, J. Mei, R. Huang, and P. Wang, 2022, Elastic FWI for large impedance contrasts: Second International Meeting for Applied Geoscience & Energy, SEG/AAPG, Expanded Abstracts, 3686–3690, https://doi.org/10.1190/image2022-w17-02.1.